

Kinetics investigation of NO + CO reaction on La–Sr–Mn–O perovskite-type mixed oxides

A.A. Leontiou^{a,*}, A.K. Ladavos^{a,1}, G.S. Armatas^a, P.N. Trikalitis^b, P.J. Pomonis^a

^a Department of Chemistry, University of Ioannina, Ioannina 45110, Greece

^b Department of Materials Science and Engineering, University of Ioannina, Ioannina 45110, Greece

Received 1 September 2003; received in revised form 8 December 2003; accepted 9 December 2003

Abstract

Substituted perovskite-type mixed oxides of the general formula $\text{La}_{1-x}\text{Sr}_x(\text{Mn}^{\text{III}}/\text{Mn}^{\text{IV}})\text{O}_{3\pm\delta}$ prepared by the nitrate method were examined by X-ray diffractometry (XRD) and the diffraction data were analyzed using the Rietveld refinement method. The amount of desorbed oxygen from the samples when heating in a He atmosphere was estimated with thermogravimetric O_2 /temperature programmed desorption experiments while the amount of Mn^{III} and Mn^{IV} in the samples was determined iodometrically. The substitution of La^{3+} by Sr^{2+} leads to a gradual increase of Mn^{IV} in the solids and to the transition from an oxygen excess state to an oxygen deficient one. The samples were checked as catalysts for the reaction $\text{NO} + \text{CO} \rightarrow \text{products}$ in a lab-scale plug-flow reactor between 220 and 560 °C. The reaction rate profiles were simulated using a relationship of the form $R = w_1 R_{\text{low } T} + w_2 R_{\text{high } T}$, where w_1 , w_2 the weighing coefficients for the corresponding R at low $R_{\text{low } T}$ and high temperatures $R_{\text{high } T}$. From the fitting data the true activation energies E_1 and E_2 were estimated for $R_{\text{low } T}$ and $R_{\text{high } T}$ as well as the heats of adsorption $\Delta H_{\text{ads}(\text{NO})}$ and $\Delta H_{\text{ads}(\text{CO})}$ for the NO and CO species. Finally, the values of $E_{\text{app/low } T}$ estimated from typical Arrhenius plots $\ln R = f(1/T)$ at the low temperature region are in reasonable agreement with the difference $E_1 - \Delta H_{\text{ads}(\text{NO})}$, a fact validating the results of simulation/fitting and indicating its usefulness for describing the reaction rates and estimating the kinetic and thermodynamic parameters controlling them. This methodology of simulation provides easily kinetic (activation energies) as well as thermodynamic (heats of adsorption) parameters which otherwise would necessitate differentiated experimental set-ups.

© 2003 Elsevier B.V. All rights reserved.

Keywords: Perovskites; La–Sr–Mn–O; Rietveld; NO + CO reaction; Kinetics

1. Introduction

Perovskite-type oxides of the general formula ABO_3 predominate among the mixed metal oxides, which are used in various physicochemical applications like sensors, conductors and super-conductors, photocatalysts and catalysts. The unique electrical and catalytic properties of perovskites with a lanthanide in A-position and a transition metal in B-position have rendered these solids effective for various industrial applications [1]. A great deal of interest has been devoted to manganese–lanthanum perovskites due to their unusual transport and magnetotransport properties [2]. It has also been shown that LaMnO_3 perovskite exhibited an abrupt change in conductivity as well as in magnetic sus-

ceptibility as a function of temperature close to 720 K [3]. Conductivity can be enhanced considerably by partial substitution of the lanthanide by a divalent ion. For the system $\text{La}_{1-x}\text{Sr}_x\text{MnO}_3$ the Mn ions are Mn^{III} for $x = 0$ whether an increase in x results in the creation of Mn^{IV} ions, thereby increasing conductivity. Additionally, $\text{La}_{1-x}\text{Sr}_x\text{MnO}_3$ type perovskites have been extensively used as cathode materials in ZrO_2 based solid oxide fuel cells [4]. These materials have also been considered of great interest concerning their utilization as catalysts for exhaust gas depollution processes and their catalytic performance has been compared with that of noble metals [5,6]. Their catalytic activity has been studied for various oxidation and reduction processes. The catalysts LaMO_3 , $\text{La}_{1-x}\text{Sr}_x\text{MO}_3$ ($M = \text{Fe}, \text{Co}, \text{Mn}, \text{Cr}$) and $\text{LaMn}_{0.99}\text{Pt}_{0.01}\text{O}_3$ prepared via various methods have shown a noticeable activity for the catalytic reduction of NO by CO [7–9] despite their low specific surface area.

LaMnO_3 is a non-stoichiometric compound [10] in which, in order to reduce the static Jahn–Teller distortion of

* Corresponding author. Tel.: +32-651098361; fax: +32-651098795.

E-mail address: me00717@cc.uoi.gr (A.A. Leontiou).

¹ Present address: Department of Farm Organisation and Management, University of Ioannina, Agrinio 30100, Greece.

Mn^{III}, cationic vacancies are created, accompanied by the formation of Mn^{IV} ions and of an oxygen excess [11–14]. The substitution of the trivalent metal ion in A-position (La) with a divalent metal cation (Sr) is accompanied by the modification of the oxidation state of metal cation in B-position, thus leading to the formation of structural defects and oxygen excess is demoted. As a result by increasing the degree of substitution x the amount of released oxygen decreases due to a decrease of cation vacancies concentration [15–17]. It can be concluded that the substitution of a bivalent cation for La³⁺ is accompanied by oxidation of the B cation (Mn). The system LaMnO_{3+δ} is one of the few perovskite systems that display apparent oxygen excess. This sample, prepared by calcination of the corresponding oxides in air at 1473 K, proved to have a composition of LaMnO_{3.12} [10] while similar δ values for lanthanum manganates were also reported elsewhere [11,18–20]. Neutron diffraction studies revealed that oxygen excess in LaMnO_{3.12} is accommodated by vacancies at the A- and B-sites with partial elimination of La (as La₂O₃), the composition of the perovskite being La_{0.94}V_{0.06}Mn_{0.98}V_{0.02}O₃, where V is a cation vacancy. The non-stoichiometry in LaMnO_{3+δ} can also be modified by partial substitution of A and B cations [21–23]. For Sr_{*x*}La_{1-*x*}MnO_{3+δ} perovskites ($x = 0.0$ – 0.5) it has been found [23] oxygen non-stoichiometry in the temperature range from 873 to 1273 K.

In the present work, eight perovskite-type mixed oxides of general formula La_{1-*x*}Sr_{*x*}MnO_{3±δ} ($x = 0.00, 0.15, 0.30, 0.40, 0.60, 0.70, 0.80$ and 0.90) were prepared, characterized and tested as catalysts for the reduction of NO by CO. The aim of the work was to investigate the influence of the substitution of trivalent La by divalent Sr on the oxygen storage properties and the catalytic properties of these materials. The determination of the oxidation state of Mn was also carried out in order to correlate the results with the above properties. Besides, the simulation of kinetic results enabled us to calculate the corresponding activation energies and the heats of adsorption of both reactants NO and CO on the eight samples tested.

2. Experimental

2.1. Preparation of materials

The solids of the general formula La_{1-*x*}Sr_{*x*}MnO_{3±δ} for various values of x ($x = 0.0, 0.15, 0.3, 0.4, 0.6, 0.7, 0.8, 0.9$) were prepared according to the nitrate method as follows: calculated amounts of La(NO₃)₃·6H₂O (Fluka), Sr(NO₃)₂ (Ferak) and Mn(NO₃)₂·4H₂O (Riedel-de Haën) were mixed and heated up to 400 °C at a rate of 3 °C/min. After no NO₂ fumes were visible, the samples were further heated for 4 h at 900 °C at atmospheric conditions. At the end of this step, the mixtures were cooled and after grinding in an agate mortar they were heated again for another 4 h at 1000 °C. The solids were then slowly cooled to room temperature and stored for further use. The obtained materials with some of their properties are shown in Table 1.

2.2. Characterization of the solids

2.2.1. XRD data and Rietveld analysis

Powder XRD diffraction analysis was carried out using a BRÜKER D8 ADVANCE system employing Cu K α radiation ($\lambda = 1.5418$ Å). The samples were placed in quartz sample holders and the step scans were taken over the range of 2θ angles from 10 to 80° in steps of 0.02° (2θ). The XRD patterns shown in Fig. 1 were assigned using the Joint Committee on Powder Diffraction Standards (JCPDS) database.

The identified crystal phases are included in Table 1.

The diffraction data were analyzed by using the Rietveld powder diffraction profile-fitting technique which was used to refine the structure and to determine the parameters of crystal structure. Typical diagrams for two samples are shown in Fig. 2 while the total results are included in Table 2.

2.2.2. Surface area measurements

The specific surface area of the prepared materials was checked by N₂ adsorption (BET) at 77 K using a single point Carlo-Erba Sorpty 1750 apparatus. All samples before

Table 1

Prepared solids, detected crystal phases (XRD), amount of oxygen desorbed (thermogravimetric O₂/TPD) in $\mu\text{mol/g}$ and specific surface area (BET) in m^2/g

Solid composition	Crystal phases	Oxygen desorbed ($\mu\text{mol/g}$ of sample)	Specific surface area (m^2/g)
LaMnO _{3±δ}	La _{0.9} MnO _{3±x} ^a /La(OH) ₃	109.6	2.3
La _{0.85} Sr _{0.15} MnO _{3±δ}	La _{0.79} Sr _{0.21} MnO _{3±x} ^a /La(OH) ₃	62.9	2.1
La _{0.7} Sr _{0.3} MnO _{3±δ}	La _{0.69} Sr _{0.31} MnO _{3±x} ^a /La(OH) ₃	35.0	2.1
La _{0.6} Sr _{0.4} MnO _{3±δ}	La _{0.7} Sr _{0.3} MnO _{3±x} ^a /La(OH) ₃ /Sr ₂ MnO ₄	33.0	2.0
La _{0.4} Sr _{0.6} MnO _{3±δ}	La _{0.57} Sr _{0.43} MnO _{3±x} ^a /Sr ₂ MnO ₄	50.2	2.2
La _{0.3} Sr _{0.7} MnO _{3±δ}	Mixture of SrMnO _{3±x} and LaMnO _{3±x} ^a /Sr ₂ MnO ₄	47.0	2.0
La _{0.2} Sr _{0.8} MnO _{3±δ}	Mixture of SrMnO _{3±x} and LaMnO _{3±x} ^a /Sr ₂ MnO ₄	70.1	2.1
La _{0.1} Sr _{0.9} MnO _{3±δ}	Mixture of SrMnO _{3±x} and LaMnO _{3±x} ^a /Sr ₂ MnO ₄	234.3	2.0

^a Main crystal phase.

Table 2

The percentage of the observed crystal phases as calculated by Rietveld analysis and the unit cell parameters of the perovskite phase

Solid (nominal composition)	Observed phases			Unit cell parameters of perovskite (Å)			
	La(OH) ₃	Sr ₂ MnO ₄	Perovskite	Space group	<i>a</i>	<i>b</i>	<i>c</i>
LaMnO _{3±δ}	13%	Not present	87% La _{0.9} MnO _{3±x}	<i>R</i> -3 <i>c</i>	5.46904	5.46904	5.469040
La _{0.85} Sr _{0.15} MnO _{3±δ}	11%	Not present	89% La _{0.79} Sr _{0.21} MnO _{3±x}	<i>R</i> -3 <i>c</i>	5.51530	5.51530	13.34219
La _{0.7} Sr _{0.3} MnO _{3±δ}	13%	Not present	87% La _{0.69} Sr _{0.31} MnO _{3±x}	<i>R</i> -3 <i>c</i>	5.51288	5.51288	13.34476
La _{0.6} Sr _{0.4} MnO _{3±δ}	10%	5%	85% La _{0.70} Sr _{0.30} MnO _{3±x}	<i>R</i> -3 <i>c</i>	5.50800	5.50800	13.33977
La _{0.4} Sr _{0.6} MnO _{3±δ}	Not present	15%	85% La _{0.57} Sr _{0.43} MnO _{3±x}	<i>R</i> -3 <i>c</i>	5.48632	5.48632	13.31478
La _{0.3} Sr _{0.7} MnO _{3±δ} ^a	Not present	Present	Mixture of SrMnO _{3±x} and LaMnO _{3±x}				
La _{0.2} Sr _{0.8} MnO _{3±δ} ^a	Not present	Present	Mixture of SrMnO _{3±x} and LaMnO _{3±x}				
La _{0.1} Sr _{0.9} MnO _{3±δ} ^a	Not present	Present	Mixture of SrMnO _{3±x} and LaMnO _{3±x}				

^a Due to low crystallinity of these samples Rietveld analysis was unable to be performed.

measurement were degassed at 250 °C for 4 h at *P* = 4 mbar. The obtained results are included in Table 1.

2.2.3. Thermogravimetric O₂/TPD analysis

Temperature-programmed desorption (TPD) experiments for the prepared solids were conducted using a NETZCH STA 449C thermobalance. The detailed description of the experimental procedure has been published previously [22]. Briefly, each sample (~70 mg) was placed in an alumina crucible and Al₂O₃, which undergoes no thermal change in

the temperature range of the experiment, was placed in an identical crucible as a reference sample. The temperature of the samples was measured by thermocouples of platinum and of platinum plus 10% rhodium. The sample was first pretreated in He stream (20 ml/min) from ambient temperature up to 700 °C. Following this, it was cooled to 550 °C in the same atmosphere and then it was kept under O₂ flow (20 ml/min) for 1 h. After cooling at 70 °C, a gas flow of He (10 ml/min) was passed through the sample subjected to

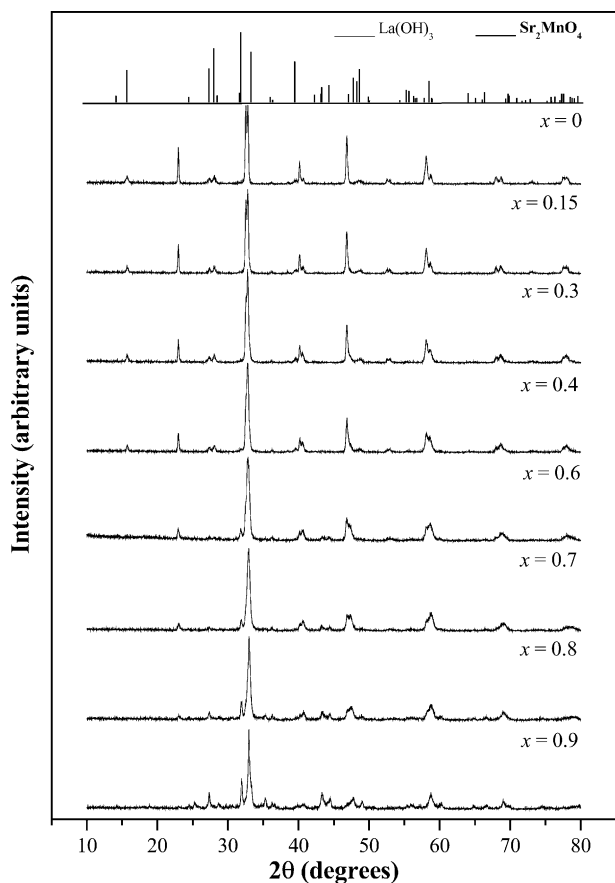


Fig. 1. XRD diffractograms of the solids and the peaks of the determined phases La(OH)₃ (grey lines) and Sr₂MnO₄ (black lines) according to the JCPDS database. The rest peaks correspond to the perovskite phase.

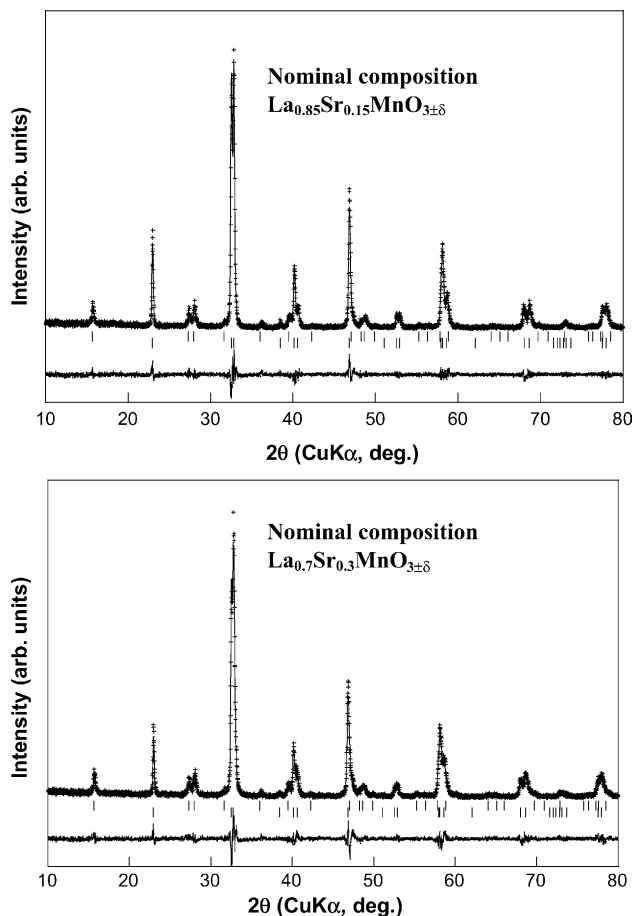


Fig. 2. Results of the Rietveld refinement for the solids indicated. The curves at the bottom correspond to the difference between the experimental and the calculated values of X-ray data.

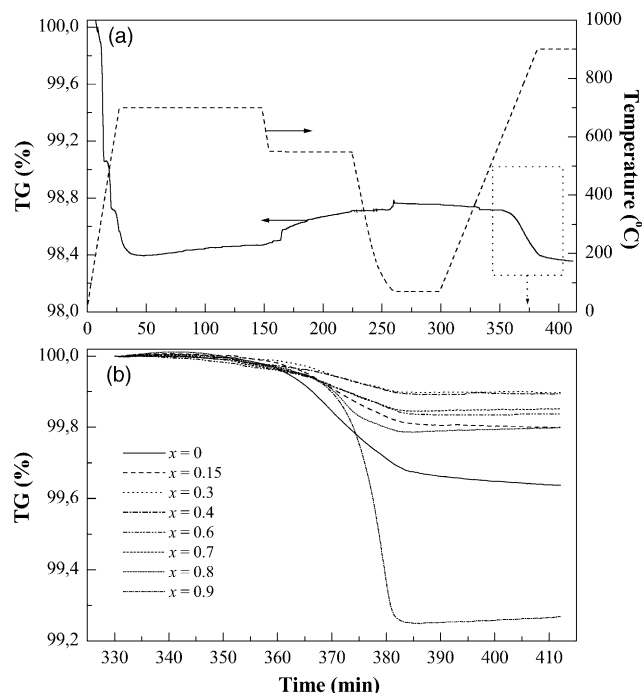


Fig. 3. A typical TG curve with the temperature program of: (a) the TPD O_2 experiments and (b) the temperature profiles of all samples during the last step of the procedure.

heating until 900°C . A weight loss is observed during the last calcination step of the procedure which corresponds to oxygen desorption. The results are summarized in Fig. 3.

2.2.4. Iodometric determination of Mn^{III} and Mn^{IV} state

An adaption of the iodometry method described by Vogel [24] was used for the determination of the amount of Mn^{III} and Mn^{IV} . As originally suggested, Mn^{III} and Mn^{IV} are reduced with excess hydrochloric acid to the divalent state as follows: Into a 500 ml flask, 30 ml of 0.5 N HCl and 25 ml of 0.16 M KI solution, excess in both cases, were added. The flask was warmed to about 50°C and a weighed amount of the sample (~ 0.2 g) was added. Chlorine is produced by the reactions:

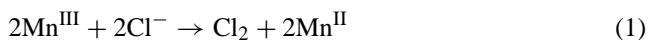


Table 3

Iodometry results, calculated coefficients of manganese and oxygen in the formula $La_{1-x}Sr_xMn_y(III)Mn_{1-y}(IV)O_{3\pm\delta}$ and the absolute values $|\delta|$

x	Mn_I (mol/100 g)	Mn_{ox} (equivalent/100 g)	Coefficients for elements in formula			$ \delta $
			Mn^{III}	Mn^{IV}	O	
0	0.4135	0.4818	0.83	0.17	3.083	0.083
0.15	0.4271	0.5107	0.80	0.20	3.023	0.023
0.3	0.4416	0.5499	0.75	0.25	2.972	0.028
0.4	0.4518	0.5986	0.68	0.32	2.962	0.038
0.6	0.4738	0.6587	0.61	0.39	2.895	0.105
0.7	0.4856	0.7131	0.53	0.47	2.884	0.116
0.8	0.4980	0.7368	0.52	0.48	2.840	0.160
0.9	0.5110	0.7412	0.55	0.45	2.775	0.225

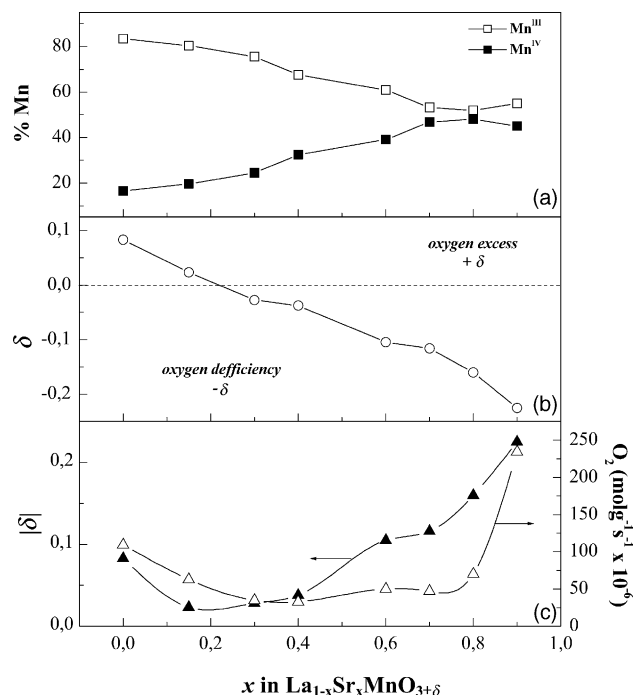
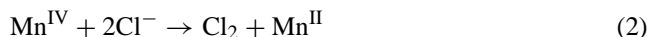


Fig. 4. The percentage values of: (a) Mn^{III} and Mn^{IV} , (b) δ values found by iodometric analysis of $La_{1-x}Sr_xMn_y(III)Mn_{1-y}(IV)O_{3\pm\delta}$ samples and (c) both values of $|\delta|$ and of the desorbed O_2 from TPD experiments as a function of the degree of substitution x .



The produced chlorine reacts with the surplus of potassium iodide solution and iodine is formed. After the sample dissolved completely, the flask was cooled in a dark place and its content was titrated with standard thiosulfate solution 0.02 N using starch as indicator. The results are given in Table 3 as equivalent Mn_{ox} per 100 g of sample. The same results are shown in Fig. 4 as a function of substitution x of La by Sr in $La_{1-x}Sr_xMnO_{3\pm\delta}$.

2.2.5. Catalytic activity

The catalytic activity of the perovskite series $La_{1-x}Sr_xMnO_{3\pm\delta}$ was studied for the reduction of nitric oxide by carbon monoxide using a bench scale plug-flow reactor

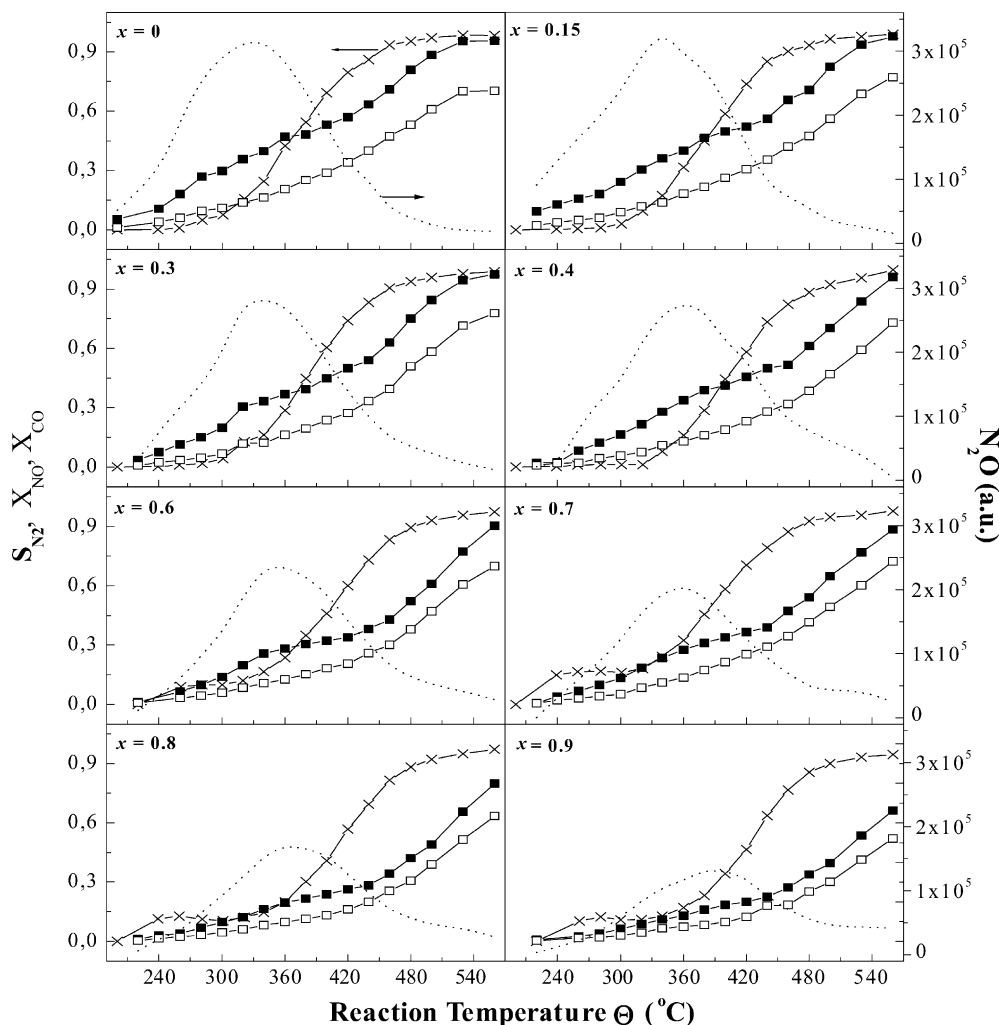


Fig. 5. Temperature profiles for NO (■) and CO (□) conversion, selectivity to N₂ (left hand axis (+)) and production of N₂O in arbitrary units (right hand axis, dash line) for the La_{1-x}Sr_xMnO_{3±δ} catalysts.

(PFR), under atmospheric pressure. The reactor was connected to a gas chromatograph (GC) for analysis of reactants and products equipped with a TCD with He as a carrier gas and connected to a PC for data acquisition. Briefly a gas mixture of NO (2%), CO (2%) and He (96%) was fed at a flow rate of 100 ml/min through the catalyst bed containing a constant amount of the catalyst ($w = 200$ mg). Flow rates were adjusted using MKS Type 247 mass flow controllers. The system was heated externally via a tubular furnace, regulated by a SUR BERLIN controller, using a thermocouple placed in the centre of the catalyst bed, within ± 2 °C. A 10-port valve enables sampling of 1 cm³ of reactants and products for analysis using two columns, one Porapac Q for N₂O and CO₂ and one molecular sieve 13× for N₂, NO and CO. The procedure of the analysis was similar to that described in [33]. The catalysts were tested in the temperature region of 220–560 °C and from the data obtained the degrees of conversion and the reaction rates were calculated. The temperature profiles for the percentage conversion of NO and CO, the selectivity towards N₂ as

well as the production of N₂O in arbitrary units are shown in Fig. 5.

3. Results

3.1. Catalysts characterization

3.1.1. XRD data and Rietveld analysis

The XRD patterns of the catalysts summarized in Fig. 1, were compared to the relevant data in the Data Bank available in the diffractometer. The results reveal that a pure perovskite structure has not been formed. The formation of such a pure phase for materials prepared via ceramic method necessitates a calcination at higher temperatures than 1000 °C employed in the present case. Furthermore, it is well known that a single phase perovskite cannot be formed for the tested system La_{1-x}Sr_xMnO_{3±δ} with the conventional solid state method for $x > 0.6$ [17,25,26]. In the case of the first samples of the series ($x \leq 0.4$) apart from the perovskite-type

structure, $\text{La}(\text{OH})_3$ was also detected. The exact composition of the perovskite phase for each sample is shown in Table 1. With further substitution of La by Sr ($x \geq 0.4$), in addition to the major perovskite phase, a second phase of Sr_2MnO_4 was observed. For higher degrees of substitution, $\text{La}(\text{OH})_3$ is not detected anymore. In the present study for $x \geq 0.7$ a mixture of $\text{LaMnO}_{3\pm x}$ and $\text{SrMnO}_{3\pm x}$ is detected and the phase Sr_2MnO_4 is also present. In Fig. 1, the peak positions of the phases $\text{La}(\text{OH})_3$ and Sr_2MnO_4 are denoted in the top by vertical bars while the rest of the peaks correspond to the major perovskite phase.

A Rietveld refinement of the obtained XRD data was made using a relevant computer program [27] for quantitative phase analysis of the multicomponent systems. Typical results for two of the tested samples are shown in Fig. 2 where the experimental and calculated XRD patterns are marked with (+) symbols and by solid lines, respectively. The satisfactory matching of the experimental with the calculated values of XRD data can be evaluated from the curve presented at the bottom of each figure which corresponds to the difference between these two quantities. The corresponding percentages of the crystal phases are included in Table 2 together with the unit cell parameters for the main perovskite phase (rhombohedral $R\bar{3}c$ for $x = 0$ and hexagonal $R\bar{3}c$ for $x \geq 0.15$). The values of a and c cell parameters (\AA) versus the degree of substitution x are plotted in Fig. 6. We observe that both parameters decrease with increasing Sr content in the samples in accordance with other data reported in the literature for similar samples [28]. The values for the first sample of the series ($x = 0$) are only pointed in the graph because the rhombohedral lanthanum-deficient phase $\text{La}_{0.88}\text{MnO}_{2.92}$ cannot be connected and therefore compared with the rest hexagonal perovskite phases.

3.1.2. Thermogravimetric O_2 /TPD analysis

The applied temperature program and a typical TG curve are presented in Fig. 3a while the TPD profiles of all the samples during the last step where the desorption of oxygen

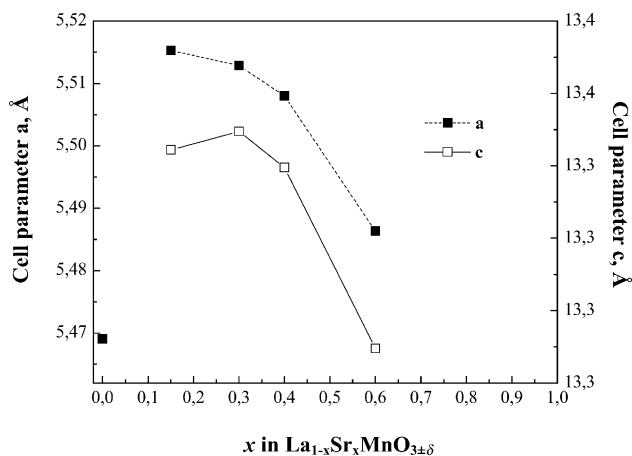


Fig. 6. The values of a , c cell parameters (\AA) vs. the degree of substitution x for the first five samples of the series.

takes place are shown in Fig. 3b. During the first calcination step, from room temperature to 700°C in He atmosphere (flow of $20\text{ cm}^3/\text{min}$), a weight loss is observed corresponding to the desorption of oxygen and probably other absorbed molecules like water and carbon dioxide. In the second step, the temperature is kept to 700°C , always under He flow, and the TG curve remains constant. In the third step, the temperature is lowered to 550°C and the He flow is switched to O_2 ($20\text{ cm}^3/\text{min}$). At this stage a sharp increase of the weight is observed due to O_2 adsorption. In the fourth step, the temperature is lowered to 70°C , under O_2 atmosphere, and kept there for 20 min. Further increase of the weight is observed during this step as expected due to further O_2 adsorption. Finally, at the fifth and last calcination step from 70 to 900°C under helium flow, a weight loss is observed (Fig. 2b) which corresponds to oxygen desorption. The amount of desorbed oxygen, during this last calcination step is reported in Table 1 as micromoles of oxygen desorbed per gram of solid. We observe that for low degrees of substitution of La by Sr the amount of desorbed oxygen decreases as the Sr content of the sample increases while for higher degrees of substitution ($x > 0.7$) the desorbed oxygen increases noticeably reaching the maximum value for $x = 0.9$. As shown in Fig. 3b, the amount of desorbing oxygen for the catalyst $\text{La}_{0.1}\text{Sr}_{0.9}\text{MnO}_{3\pm\delta}$ is more than double of the corresponding amount for the catalyst $\text{LaMnO}_{3\pm\delta}$ containing no Sr at all.

3.1.3. Iodometric analysis

The content of Mn^{III} and Mn^{IV} can be calculated [29] from the titration results (Mn_{ox}) knowing the total manganese content (Mn_{t}) from the preparation data of the solids from Eqs. (3) and (4):

$$\text{Mn}_{\text{t}} = n_1\text{Mn}^{\text{III}} + n_2\text{Mn}^{\text{IV}} \quad (3)$$

$$\text{Mn}_{\text{ox}} = n_1\text{Mn}^{\text{III}} + 2n_2\text{Mn}^{\text{IV}} \quad (4)$$

it can be derived that

$$\text{Mn}^{\text{III}} = 2\text{Mn}_{\text{t}} - \text{Mn}_{\text{ox}} \quad (5)$$

$$\text{Mn}^{\text{IV}} = \text{Mn}_{\text{ox}} - \text{Mn}_{\text{t}} \quad (6)$$

The resulting coefficients for the manganese in the formula $\text{La}_{1-x}\text{Sr}_x\text{Mn}_y^{\text{III}}\text{Mn}_{1-y}^{\text{IV}}\text{O}_{3\pm\delta}$ are reported in Table 3. We observe that the percentage of $\text{Mn}(\text{IV})$ increases as La is substituted by Sr reaching the value of about 50% in high degrees of substitution. Fig. 4a presents the calculated percentage values of Mn^{III} and Mn^{IV} in the solids versus the degree of substitution of La for Sr. The amount of Mn^{III} declines as x increases while Mn^{IV} increases with x until the value of about 50%. Oxygen content was evaluated from the cation composition based on the charge neutrality condition. In Fig. 4b, δ values found by the above-described analysis are plotted against the degree of strontium substitution x . The transition from an oxygen excess state to an oxygen deficiency one is apparent as shown by the decrease of δ values as a function of Sr substitution. The positive

values of δ for the first two samples ($x < 0.2$) are replaced by negative ones for the rest six samples of the examined series ($0.2 < x < 0.9$). This behavior is also reported in Table 3 in the form of the oxygen coefficient in the formula $\text{La}_{1-x}\text{Sr}_x\text{Mn}_y^{\text{III}}\text{Mn}_{1-y}^{\text{IV}}\text{O}_{3\pm\delta}$.

3.2. Catalytic studies

The solids $\text{La}_{1-x}\text{Sr}_x\text{MnO}_{3\pm\delta}$ were active for the interconversion of NO and CO between 220 and 560 °C showing a significant activity in this temperature range. In Fig. 5, apart from the temperature profiles for the percentage conversion of NO (X_{NO}) and CO (X_{CO}), the N_2 formation and the N_2O production in arbitrary units are also shown versus temperature. At temperatures higher than about 480–500 °C the N_2 selectivity is always 95–100%. It is noted that the production of N_2O starts at low temperatures and reaches a maximum at 340–380 °C depending on the composition of the sample and at higher temperatures its production decreases. We observe that the production of N_2O decreases as the degree of substitution of Sr for La increases while the peak is shifted to higher reaction temperatures.

The integral reaction rates of NO consumption ($\mu\text{mol}/(\text{g s})$) at $T = 300, 360, 420$ and 500 °C as well as the corresponding rates of CO consumption, both as a function of the catalyst composition, are shown in Fig. 7a and b, respectively. It is obvious that $\text{LaMnO}_{3\pm\delta}$ is the most active catalyst and the activity declines as Sr content increases. In the

third part of Fig. 7, the values of N_2O production in arbitrary units, read out from Fig. 5, are also plotted against x . It can be seen that the catalysts with higher Sr content produce less N_2O . Combining this with the above described iodometric results, we can say that the lower activity and lower selectivity towards N_2O , correspond to lower values of the ratio $\text{Mn}^{\text{III}}/\text{Mn}^{\text{IV}}$ as well as lower values of δ , which express the oxygen excess ($+\delta$) or deficiency ($-\delta$) in the samples (see Fig. 4). In Fig. 7c, we notice that for low temperatures (300 and 360 °C) the curves showing the N_2O production are characterized by a continuous decline while at higher temperatures (420 and 500 °C), where about the maximum production of N_2O is observed for all samples, the curves show a different trend as mentioned previously (see Fig. 5).

In Fig. 8, the variation of the ratio of the products $\text{CO}_2/(\text{N}_2 + \text{N}_2\text{O})$ is shown as a function of reaction temperature. It is observed that this ratio takes values of about unity at low temperatures and increases towards values of two as the temperature increases. We emphasize that this transition is more obvious for the last four samples of the series tested where the amount of Sr and Mn^{IV} is higher. In these catalysts, the production of nitrous oxide is less compared to the first four samples with less Sr and Mn^{IV} .

In the same Fig. 8 we have drawn Arrhenius-type plots of the form $\ln R_{\text{NO}} = f(1000/T)$ as well as $\ln R_{\text{CO}} = f(1000/T)$, where R is the observed rate of conversion in $\mu\text{mol}/(\text{g s})$. As observed from the Arrhenius-type plots, at low temperatures there is a straight-line part and from its slope the apparent activation energies in this low-temperature region ($E_{\text{app,low } T}$) can be estimated. These values are tabulated in Table 5. At this low-temperature region the ratio $\text{CO}_2/(\text{N}_2 + \text{N}_2\text{O})$ reaches values around the value of 2. Then as the temperature increases we reach the medium reaction range which is shaded in Fig. 8. In this medium shaded region the Arrhenius-type plots show a significantly smoother slope. It is in this region that the transition of the ratio $\text{CO}_2/(\text{N}_2 + \text{N}_2\text{O})$ takes place from 1 towards 2. Then at higher temperatures the Arrhenius lines return to a steeper slope. In this temperature range the ratio $\text{CO}_2/(\text{N}_2 + \text{N}_2\text{O})$ reaches values around 2. These results will be discussed extensively next.

4. Discussion

As shown by the determination of the reaction rates, the substitution of lanthanum by strontium decreases the catalytic activity. Additionally, iodometric analysis showed that the increase of Sr content leads to a transition from an oxygen excess state to an oxygen deficient one. There is an obvious similarity between the graphs depicting the reaction rates for the NO and CO elimination versus the degree of substitution (Fig. 7a and b) on one hand and the graph of the parameter δ decreasing linearly with x (Fig. 4b) on the other. By increasing x the oxygen vacancies in the samples increase and the catalytic activity declines accordingly. In

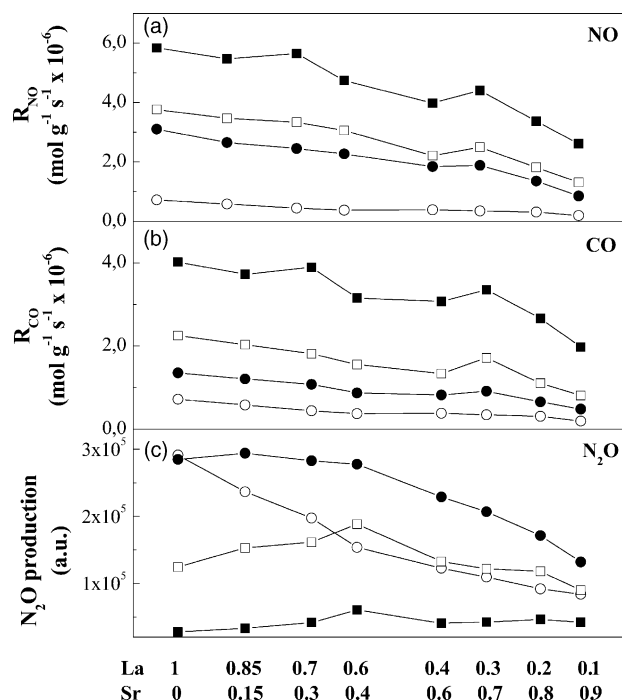


Fig. 7. The conversion rates of: (a) the reactants NO and (b) CO as a function of substitution x of La by Sr at $\theta = 300$ (○), 360 (●), 420 (□) and 500 °C (■). In the lower part (c), the production of N_2O (a.u.) from the data in Fig. 4 is also shown as a function of x at the same temperatures.

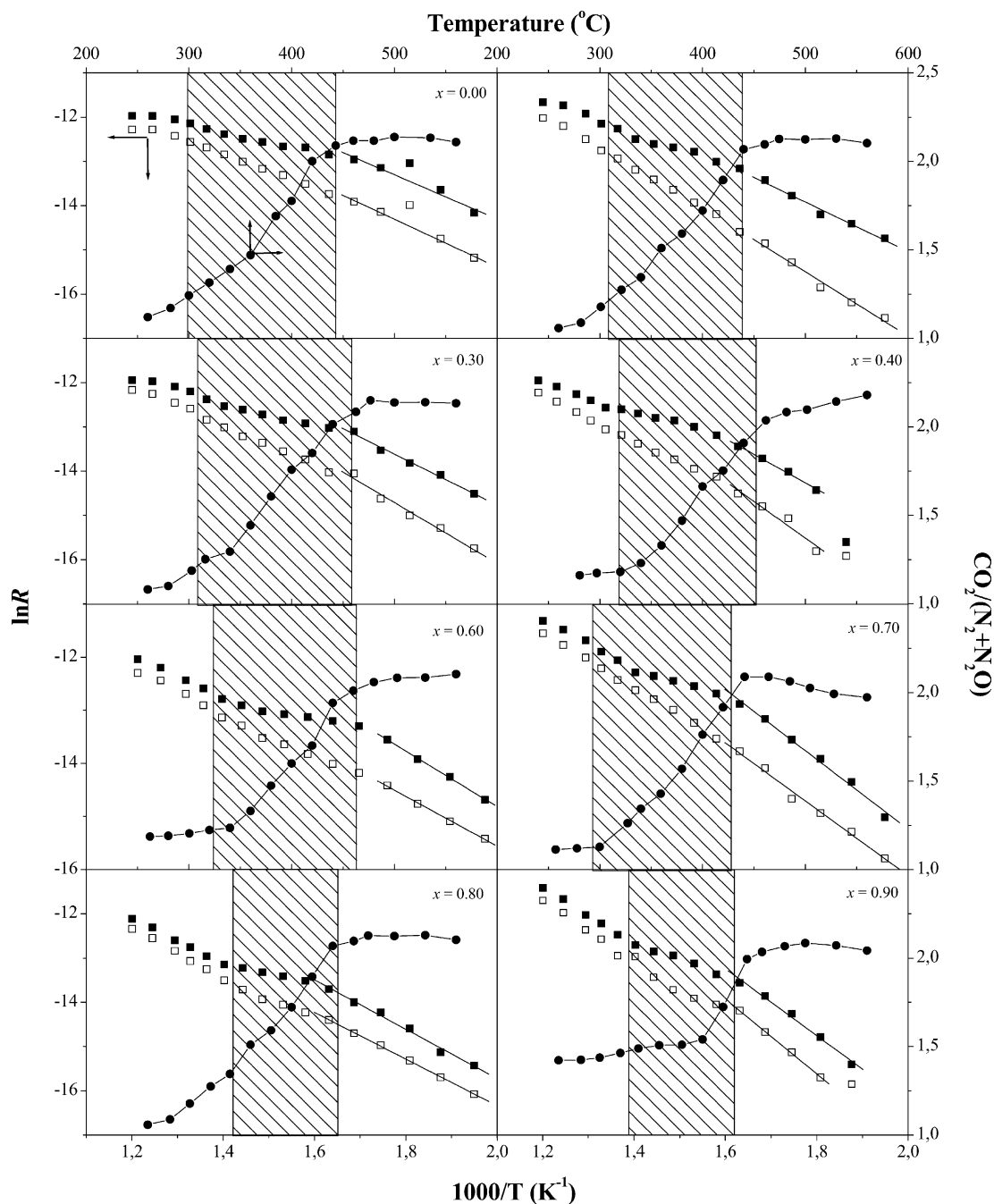


Fig. 8. The ratio of the products $\text{CO}_2/(\text{N}_2 + \text{N}_2\text{O})$ (●) as a function of reaction temperature (left hand and upper axes) and the Arrhenius plots $\ln R_{\text{NO}}$ (■) and $\ln R_{\text{CO}}$ (□) vs. $1000/T$ (right hand and lower part axes).

other words, samples deficient in oxygen (low δ values) show lower activity in catalytic experiments compared to the ones with oxygen excess (high δ values). This should be due to the fact that the oxygen deficient samples retain a part of the oxygen produced by the decomposition of NO ($\text{NO}_{\text{ads}} \rightarrow \text{N}_{\text{ads}} + \text{O}_{\text{ads}}$) thus inhibiting all the reaction steps requiring mobile oxygen in order to take place. These reactions are described next. So, the smaller the value of δ is, the lower the interconversion of NO and CO proves to be.

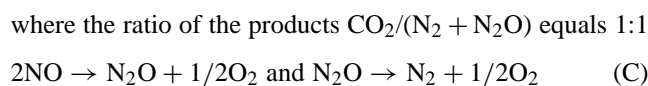
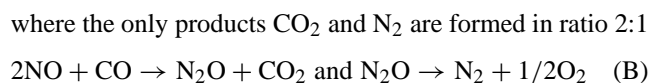
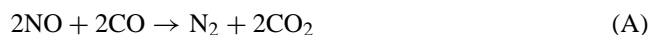
In Fig. 4c, two parameters related to the presence of oxygen in the samples and determined by different methods are shown as a function of the substitution x : first, the absolute value of δ ($|\delta|$) as derived by the results taken from iodometric analysis and second the amount of desorbed oxygen as determined by O_2/TPD experiments. Obviously, these two curves show close similarity. For low values of x , the samples with oxygen excess probably desorb a part of this excess during the O_2/TPD experiments except for the suprafacial adsorbed oxygen, while for high degrees of x , the increased values

of desorbed oxygen are due to both *suprafacial* and *oxygen desorbed from the bulk* of the solid which had occupied the inner anion vacancies created by substitution of Sr for La.

The catalytic reduction of nitric oxide by carbon monoxide on perovskites [30–32] has been described to proceed according to the following elementary surface processes:



These reactions can be expressed by the following three main routes [31–33]:



The last route (C) includes only nitric oxide transformation and can take place on top of any one of the previous routes.

Which route is actually followed can be verified by checking the ratio of the products. As it has been reported previously for similar materials [33], for low reaction temperatures ($\theta \leq 350^\circ\text{C}$) and low degrees of NO and CO conversion (<5%), the ratio of $\text{CO}_2/(\text{N}_2 + \text{N}_2\text{O})$ takes

values around and above unity (Fig. 8), which means that route (B) predominates, but also route (C) takes place. Then at higher reaction temperatures (above $\sim 350^\circ\text{C}$) a gradual change from values $\text{CO}_2/(\text{N}_2 + \text{N}_2\text{O}) \approx 1$ to ≈ 2 is observed. This transition from route (B) to route (A) indicated/covered by the shaded area in Fig. 7 has been completed at $\theta \geq 450^\circ\text{C}$. From this point onwards, only route (A) takes place. The same behavior was observed in other works too [34,31] where it was suggested that the catalytic transformation following route (B) at low temperatures is controlled by oxygen generated from the decomposition of NO described by reaction (b) while at high temperatures where it follows route (A) is controlled by reaction (d). The higher amount of N_2 in the middle transition rate (Fig. 5) shows that route (C) does not occur extensively while at higher temperatures the decomposition of N_2O takes place according to reaction $\text{N}_2\text{O} \rightarrow \text{N}_2 + 1/2\text{O}_2$ producing N_2 .

The two reaction rate components, the first at low temperature ($R_{\text{low } T}$) and the second at higher temperature ($R_{\text{high } T}$), can be expressed by the following equations:

$$R_{\text{low } T} = k_1 \theta_{\text{NO}} \quad (7)$$

$$R_{\text{high } T} = k_2 \theta_{\text{CO}} \theta_{\text{O}} \quad (8)$$

where θ is the corresponding surface coverage.

The total reaction rate is then expressed by the sum:

$$R_{\text{total}} = w_1 R_{\text{low } T} + w_2 R_{\text{high } T} \quad (9)$$

where w_1 , w_2 the weighing coefficients for routes (B) and (A), respectively, that can be estimated precisely from the ratio $\text{CO}_2/(\text{N}_2 + \text{N}_2\text{O})$ (see Fig. 7). The w_1 values are listed in Table 4 for all tested samples in the whole range of reaction temperature.

Then the reaction rates can be described by the relationships

$$R_{\text{low } T} = k_1 \theta_{\text{NO}} = k_1 \frac{K_{\text{NO}} P_{\text{NO}}}{1 + K_{\text{NO}} P_{\text{NO}}} \quad (10)$$

Table 4

The values of the weighing coefficient w_1 estimated from the ratio $\text{CO}_2/(\text{N}_2 + \text{N}_2\text{O})$ in the whole range of temperature reaction for the eight catalysts

θ ($^\circ\text{C}$)	x							
	0.0	0.15	0.3	0.4	0.6	0.7	0.8	0.9
260	0.99999	0.99979	0.99999	0.99999	0.99999	0.85612	0.98540	1.00000
280	0.71371	0.91369	0.94679	0.47197	0.99999	0.82612	0.97607	1.00000
300	0.79225	0.62526	0.9123	0.47602	0.87156	0.99999	0.95068	0.90756
320	0.68684	0.66367	0.74063	0.49236	0.93896	0.71609	0.99999	0.86562
340	0.59047	0.67422	0.60163	0.44915	0.91546	0.65581	0.90942	0.52865
360	0.50052	0.40454	0.63681	0.37124	0.75749	0.60901	0.95634	0.61393
380	0.26335	0.33325	0.47414	0.28085	0.55665	0.39341	0.74414	0.79826
400	0.22368	0.23274	0.33193	0.18082	0.41077	0.22371	0.67049	0.75511
420	0.07492	0.12246	0.22277	0.14175	0.30877	0.11211	0.40828	0.53149
440	0.07189	0.02854	0.16410	0.08270	0.10912	0.11347	0.09270	0.40072
460	0.01131	0.03893	0.07540	0.02358	0.06096	0.06215	0.08565	0.26740
480	0.01078	0.03992	0.05308	0.03658	0.02823	0.04432	0.08365	0.24427
500	0.09259	0.00222	0.08253	0.04167	0.03714	0.08997	0.20627	0.20509
530	0.10078	0.01879	0.01752	0.01015	0.01209	0.07849	0.12034	0.21520
560	0.01522	0.01221	0.01716	0.07369	0.03817	0.07542	0.02729	0.23765

$$R_{\text{high } T} = k_2 \theta_{\text{CO}} \theta_{\text{O}} = k_2 \frac{K_{\text{CO}} P_{\text{CO}} K_{\text{O}} P_{\text{O}}}{(1 + K_{\text{CO}} P_{\text{CO}} + K_{\text{O}} P_{\text{O}})^2} \quad (11)$$

Considering that $K_{\text{NO}} P_{\text{NO}} \ll 1$, the relationship (10) is reduced to:

$$R_{\text{low } T} = k_1 K_{\text{NO}} P_{\text{NO}} \quad (12)$$

In Eq. (11), the term P_{O} is not accessible and in order to express it via other terms that can be calculated, we follow the oncoming procedure. At high temperatures, where the second term of Eq. (9) refers to, the ratio $d\theta_i/dT$ equals zero and therefore the rates $R_{\text{low } T}$ and $R_{\text{high } T}$ are equal. This leads to the expression:

$$\begin{aligned} R_{\text{low } T} = R_{\text{high } T} &\Rightarrow k_1 \theta_{\text{NO}} = k_2 \theta_{\text{CO}} \theta_{\text{O}} \Rightarrow \theta_{\text{O}} \\ &= \frac{k_1 \theta_{\text{NO}}}{k_2 \theta_{\text{CO}}} = \frac{k_1 K_{\text{NO}} P_{\text{NO}}}{k_2 K_{\text{CO}} P_{\text{CO}}} \end{aligned} \quad (13)$$

Relationship (11) is then reduced to the following expression

$$R_{\text{high } T} = k_2 \frac{K_{\text{CO}} P_{\text{CO}} (k_1 K_{\text{NO}} P_{\text{NO}} / k_2 K_{\text{CO}} P_{\text{CO}})}{(1 + K_{\text{CO}} P_{\text{CO}} + (k_1 K_{\text{NO}} P_{\text{NO}} / k_2 K_{\text{CO}} P_{\text{CO}}))^2} \quad (14)$$

Finally, the total reaction rate is expressed by Eq. (15):

$$\begin{aligned} R_{\text{total}} = w_1 R_{\text{low } T} + w_2 R_{\text{high } T} &\Rightarrow w_1 (k_1 K_{\text{NO}} P_{\text{NO}}) \\ &+ w_2 \left(k_2 \frac{K_{\text{CO}} P_{\text{CO}} (k_1 K_{\text{NO}} P_{\text{NO}} / k_2 K_{\text{CO}} P_{\text{CO}})}{(1 + K_{\text{CO}} P_{\text{CO}} + (k_1 K_{\text{NO}} P_{\text{NO}} / k_2 K_{\text{CO}} P_{\text{CO}}))^2} \right) \end{aligned} \quad (15)$$

where w_1, w_2 the normalized coefficients referred to the two routes as mentioned, k_1, k_2 the rate constants; $K_{\text{NO}}, K_{\text{CO}}$ the adsorption equilibrium constants of NO and CO; $P_{\text{NO}}, P_{\text{CO}}$ the partial pressures of NO and CO.

Using the above equation we simulated the experimental results in the range of reaction temperature between 260 and 460 °C. The simulation took place using a suitable computer program written in ForTran 90/95 and based on the well-known ‘‘Simplex’’ method and the least-squared method of Levenberg-Marquardt [35–37]. The program was executed in Linux.

For the simulation of data the corresponding parameters k_1, k_2, K_{NO} and K_{CO} are expressed as follows:

$$k_1 = A_1 \exp\left(\frac{-E_1}{RT}\right) \quad (16)$$

$$k_2 = A_2 \exp\left(\frac{-E_2}{RT}\right) \quad (17)$$

$$K_{\text{NO}} = A_{\text{NO}} \exp\left(\frac{\Delta H_{\text{ads}}(\text{NO})}{RT}\right) \quad (18)$$

$$K_{\text{CO}} = A_{\text{CO}} \exp\left(\frac{\Delta H_{\text{ads}}(\text{CO})}{RT}\right) \quad (19)$$

The results of simulation for the eight examined catalysts in the high temperature region (260–460 °C) are shown in

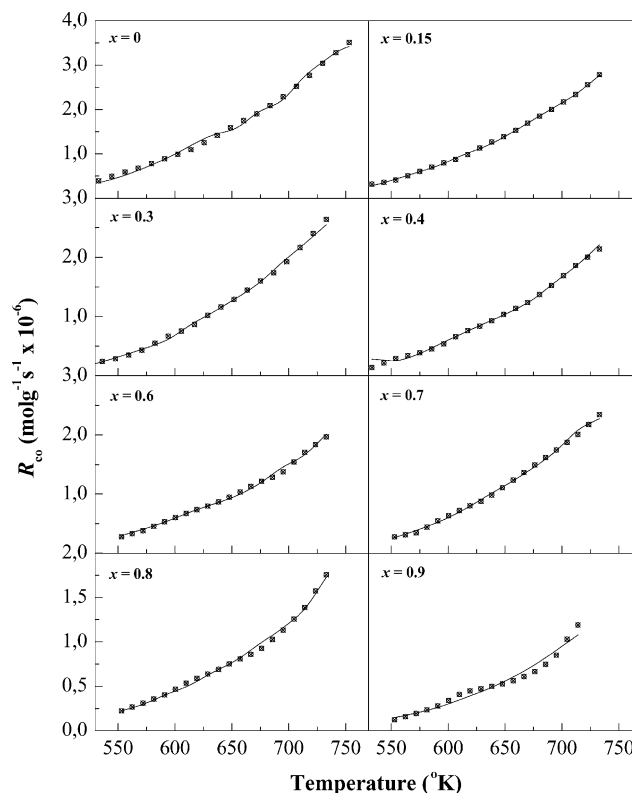


Fig. 9. Simulation results according to Eq. (15) for the high-temperature region (260–460 °C). Points: experimental data; lines: computer fitting.

Fig. 9. In this figure the points correspond to the experimental data and the solid lines correspond to the simulation by Eq. (15). The fitting of the data with the simulation was quite satisfactory as shown by the correlation coefficients (R^2) included in Table 5.

The estimated values of $A_1, A_2, A_{\text{NO}}, A_{\text{CO}}, E_1, E_2, \Delta H_{\text{ads}}(\text{NO})$ and $\Delta H_{\text{ads}}(\text{CO})$ are tabulated in Table 5.

The determined parameters $E_1, E_2, \Delta H_{\text{ads}}(\text{NO})$ and $\Delta H_{\text{ads}}(\text{CO})$ are shown as a function of degree of substitution x in $\text{La}_{1-x}\text{Sr}_x\text{MnO}_{3\pm\delta}$ in Fig. 10.

A comparison graph between the variations of the $E_{\text{app/low } T}$ values, calculated by the Arrhenius plots, and the values of the term $E_1 - \Delta H_{\text{ads}}(\text{NO})$, obtained by the simulation technique, is depicted in Fig. 11.

From Fig. 9 we observe that the simulation of experimental points with Eq. (15), into which the relationships (16), (17), (18) and (19) have been substituted, is quite satisfactory. Some systematic discrepancies are observed for the samples with high content of Sr, namely $\text{La}_{0.1}\text{Sr}_{0.9}\text{MnO}_{3\pm\delta}$, $\text{La}_{0.2}\text{Sr}_{0.8}\text{MnO}_{3\pm\delta}$ and perhaps $\text{La}_{0.3}\text{Sr}_{0.7}\text{MnO}_{3\pm\delta}$. In those samples the ‘‘knee’’ apparent in the experimental data is not so well fitted. So we shall keep some reservations for the simulation parameters describing the catalytic performance of those samples.

The variation of activation energies E_1 and E_2 as a function of Sr content is shown in Fig. 10. In the majority of the cases, E_1 is larger than E_2 . This might well reflect the fact that E_1 corresponds to the NO decomposition (see

Table 5

The values for the parameters A_1 , A_2 , E_1 , E_2 , A_{NO} , A_{CO} , $\Delta H_{ads(NO)}$ and $\Delta H_{ads(CO)}$ estimated according to the fitting of catalytic data by Eq. (15) in the region of 260–460 °C

Sample	A_1	A_2	E_1^a	E_2^a	A_{NO}	A_{CO}	$\Delta H_{ads(NO)}^a$	$\Delta H_{ads(CO)}^a$	R^2	$E_{app/low T}^a$
LaMnO _{3±δ}	1.54E4	1.16E9	131	114	3.74E-3	1.70E-6	66	28	0.9951	58
La _{0.85} Sr _{0.15} MnO _{3±δ}	1.09E4	4.65E8	129	106	2.29E-3	3.01E-7	67	34	0.9991	46
La _{0.7} Sr _{0.3} MnO _{3±δ}	1.12E4	4.77E8	127	104	2.37E-3	3.07E-7	64	33	0.9980	51
La _{0.6} Sr _{0.4} MnO _{3±δ}	8.12E3	4.54E8	126	109	1.72E-3	3.74E-7	63	29	0.9981	52
La _{0.4} Sr _{0.6} MnO _{3±δ}	2.24E3	2.81E9	108	112	5.40E-4	1.32E-6	56	19	0.9947	44
La _{0.3} Sr _{0.7} MnO _{3±δ}	3.85E3	2.18E9	113	74	1.08E-3	3.22E-10	55	34	0.9968	53
La _{0.2} Sr _{0.8} MnO _{3±δ}	1.41E3	3.30E10	93	89	1.50E-4	1.14E-3	48	50	0.9956	49
La _{0.1} Sr _{0.9} MnO _{3±δ}	1.17E3	2.99E14	63	42	1.20E-4	4.38E-16	28	49	0.9664	51

The fitting criterion R^2 is also shown. The $E_{app/low T}$ values estimated from plots $\ln R_{NO} = f(1000/T)$ at the low temperature region are shown in the right end column.

^a kJ/mol.

Eqs. (7) and (10)), while E_2 corresponds to CO oxidation (see Eqs. (8) and (11)). The first of these reactions exhibits higher activation energies compared to the second. But in general the values of E_1 and E_2 do not show appreciable changes with x and, with the exception of the last two samples ($x = 0.8$ and 0.9) for which the fitting is not so successful, remain in the range (kJ/mol) $110 < E_1 < 130$ and $105 < E_2 < 115$.

For the samples with $x = 0.8$ and 0.9 both E_1 and E_2 values decrease systematically ($E_1 = 93 \rightarrow 63$ kJ/mol and $E_2 = 89 \rightarrow 42$ kJ/mol respectively). Those values should be compared with values of activation energies estimated via similar simulation catalytic kinetic studies on three-way catalysts Pt-Rh/Al₂O₃-CeO_x [38,39]. As far as we know there are no similar simulation studies in the literature concerning ceramic mixed valence state catalysts like the present ones. These previously estimated values can be summarized as follows: Matthess et al. [38] found that the apparent activation energy for the reaction $2NO + 2CO \rightarrow$

$2CO_2 + N_2$ was $E_{app} \approx 86.6$ kJ/mol while for the reaction $CO + 1/2O_2 \rightarrow CO_2$ the corresponding value was $E_{app} \approx 112$ – 119 kJ/mol whether for the above mentioned reactions Koltsakis et al. [39] found $E_{app} \approx 70.0$ and ≈ 95.0 kJ/mol, respectively. Those values are compared satisfactorily with the E_1 and E_2 values estimated in the present study.

The variation of the heats of adsorption for NO ($\Delta H_{ads(NO)}$) and CO ($\Delta H_{ads(CO)}$) are also shown in Fig. 10. The $\Delta H_{ads(CO)}$ values are in the range of 50–60 kJ/mol while the $\Delta H_{ads(NO)}$ values appear lower in the range of 30–40 kJ/mol. Those values indicate weaker adsorption of CO on the La–Sr–Mn–O catalysts compared to NO as expected. A comparison should be made between these values and similar ones reported for the heat of adsorption of NO which on LaFeO₃ is 38 kJ/mol at surface coverage $\Theta = 0.65$ [40], on Mn₂O₃ is 117 kJ/mol [41], on La₂O₃ is 117 kJ/mol [42] and on Fe₃O₄ is 69.3 kJ/mol [43]. Nevertheless, a direct comparison is not feasible because of the

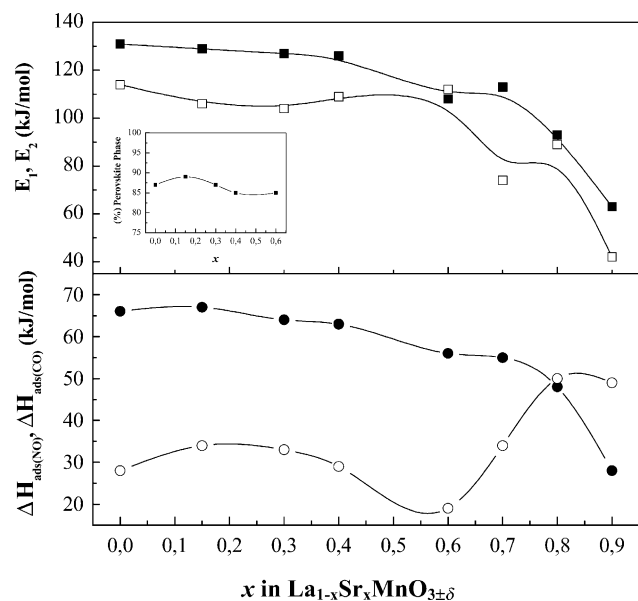


Fig. 10. The parameters E_1 (■), E_2 (□), $\Delta H_{ads(NO)}$ (●) and $\Delta H_{ads(CO)}$ (○) calculated from the simulation method as a function of the degree of substitution x . In the inset, the percentage of perovskite phase vs. x .

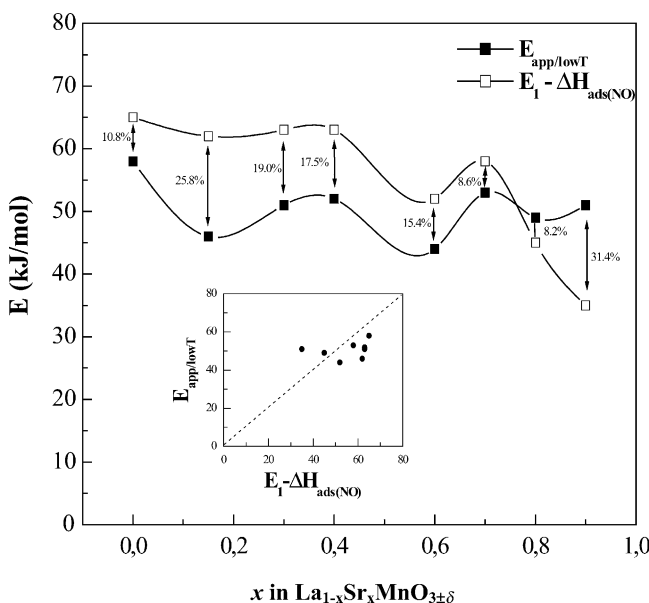


Fig. 11. The apparent activation energy $E_{app/low T}$ (■) calculated from the Arrhenius plots (Table 5) and the difference $E_1 - \Delta H_{ads(NO)}$ (□) obtained from the simulation technique as a function of the Sr substitution. In the inset, $E_{app/low T}$ vs. the difference $E_1 - \Delta H_{ads(NO)}$ is shown.

experimental differences and the difficulty in the estimation of surface coverage Θ_{NO} in each case, which affects the values of the heat of adsorption $\Delta H_{\text{ads}(\text{NO})}$.

It is apparent that the trend characterizing the determined kinetic parameters which express the catalytic activity (E_1 and E_2), shown in Fig. 10a, corresponds to a similar trend characterizing the percent of the perovskite phase determined from Rietveld analysis, shown in the inset of Fig. 10a. Such correlation cannot be made for the rest three samples of the tested series where the Rietveld analysis could not be performed.

Finally the values $E_{\text{app}/\text{low } T}$ and the difference $E_1 - \Delta H_{\text{ads}(\text{NO})}$, as shown in Fig. 11, differ in a percentage fluctuating from 8.2 to 31.4%. This reasonable agreement leads us to the conclusion that simulation/fitting can be used to describe the reaction rate satisfactorily and allows us to determine the E_i ($i = 1, 2$) and $\Delta H_{\text{ads}(j)}$ ($j = \text{NO}, \text{CO}$) parameters quite easily since otherwise a large number of complicated measurements would be demanded.

5. Conclusions

Substituted perovskite-type mixed oxides $\text{La}_{1-x}\text{Sr}_x(\text{Mn}^{\text{III}}/\text{Mn}^{\text{IV}})\text{O}_{3\pm\delta}$ show catalytic activity for the reaction $\text{NO} + \text{CO}$ in the range of 220–560 °C, which decreases linearly with the substitution of La by Sr and the gradual increase of the ratio $\text{Mn}^{\text{IV}}/\text{Mn}^{\text{III}}$. At low temperatures, the reaction proceeds via equimolecular conversion of NO and CO and the reaction rate is described by $R_{\text{low } T} = k_1\Theta_{\text{NO}}$ while at higher temperatures (>350 °C) the conversion ratio for NO:CO equals 2:1 and the reaction rate was assumed to be described by $R_{\text{high } T} = k_2\Theta_{\text{NO}}\Theta_{\text{CO}}$, where Θ_i the corresponding surface coverage of i ($i = \text{NO}, \text{CO}$). The rate R of conversion can be simulated satisfactorily using the expression $R = w_1R_{\text{low } T} + w_2R_{\text{high } T}$, where w_1, w_2 the weighing coefficients of reactions $R_{\text{low } T}$ and $R_{\text{high } T}$. The obtained results provide values for the true activation energies E_1 (for low T) and E_2 (for high T) as well as the heats of adsorption $\Delta H_{\text{ads}(\text{NO})}$ for NO and $\Delta H_{\text{ads}(\text{CO})}$ for CO. The values of E_1, E_2 and $\Delta H_{\text{ads}(\text{NO})}$ suffer a gradual drop with the addition of Sr while $\Delta H_{\text{ads}(\text{CO})}$ increases. These values are reasonably compared to previously reported data. Perhaps more important is the fact that the described method of simulation provides, using only one kind of experiment, kinetic (E_1, E_2) and thermodynamic ($\Delta H_{\text{ads}(\text{NO})}, \Delta H_{\text{ads}(\text{CO})}$) parameters which otherwise would necessitate a large number of experimental set-ups.

Acknowledgements

The authors are grateful to the Ring of the Laboratory Units and Centers of the University of Ioannina for the XRD analysis and TG experiments.

References

- [1] T. Seiyama, in: L.G. Tejuca, J.L.G. Fierro (Eds.), Properties and Applications of Perovskite-Type Oxides, Marcel Dekker, New York, 1993.
- [2] R. von Helmolt, J. Wecker, K. Samwer, K. Barner, J. Magn. Mater. 151 (1995) 411.
- [3] M.A. Pena, J.L.G. Fierro, Chem. Rev. 101 (2001) 1981.
- [4] J.H. Kuo, H.U. Anderson, D.M. Sparlin, J. Solid State Chem. 87 (1990) 55.
- [5] J. Barton, Collect. Czech. Chem. Commun. 55 (1990) 1935.
- [6] N. Guilhaume, M. Primet, J. Catal. 165 (1997) 197.
- [7] A. Kudo, M. Steinberg, A.J. Bard, A. Campion, M.A. Fox, T.E. Mallouk, S.E. Webber, J.M. White, J. Catal. 125 (1990) 565.
- [8] A. Lindstedt, D. Strömberg, M. Abul Milh, Appl. Catal. A 116 (1994) 109.
- [9] S.-T. Chen, H.-S. Weng, Ind. Eng. Chem. Res. 37 (1998) 2654.
- [10] B.C. Tofield, W.R. Scott, J. Solid State Chem. 10 (1974) 183.
- [11] N. Kamegashira, Y. Miyazaki, H. Yamamoto, Mater. Chem. Phys. 11 (1984) 187.
- [12] L.G. Tejuca, J.L.G. Fierro, J.M.D. Tascon, Adv. Catal. 36 (1989) 237.
- [13] C.N.R. Rao, J. Gopalakrishnan, K. Vidyasagar, Indian J. Chem. 23A (1984) 265.
- [14] M.T. Anderson, J.T. Vaughey, K.R. Poeppelmeier, Chem. Mater. 5 (1993) 151.
- [15] D. Ferri, L. Forni, Appl. Catal. B 16 (1998) 119.
- [16] L. Marchetti, L. Forni, Appl. Catal. B 15 (1998) 179.
- [17] T. Nitadori, S. Kurihama, M. Misono, J. Catal. 98 (1986) 221.
- [18] R.J.H. Voorhoeve, J.P. Remeica, L.E. Trimble, A.S. Cooper, F.J. Disalvo, P.K. Gallagher, J. Solid State Chem. 14 (1975) 395.
- [19] E.M. Vogel, D.W. Johnson Jr., P.K. Gallagher, J. Am. Ceram. Soc. 60 (1977) 31.
- [20] H. Taguchi, A. Sugita, M. Nagao, K. Tabata, J. Solid State Chem. 119 (1995) 164.
- [21] J. Mizusaki, N. Mori, H. Takai, Y. Yonemura, H. Minamiue, H. Tagawa, M. Dokiya, H. Inaba, K. Naraya, T. Sasamoto, T. Hashimoto, Solid State Ion. 129 (2000) 163.
- [22] A.A. Leontiou, A.K. Ladavos, T.V. Bakas, T.C. Vaimakis, P.J. Pomonis, Appl. Catal. A 241 (2003) 143–154.
- [23] J. Mizusaki, H. Tagawa, K. Naraya, T. Sasamoto, Solid State Ion. 49 (1991) 111.
- [24] A.I. Vogel, in: A Text-Book of Quantitative Inorganic Analysis Including Elementary Instrumental Analysis, Third ed., Longman, London, 1961, p. 360.
- [25] V.A. Cherepanov, L.Y. Barkhatova, V.I. Voronin, J. Solid State Chem. 134 (1997) 38.
- [26] K. Kikuchi, H. Chiba, M. Kikuchi, Y. Syono, J. Solid State Chem. 146 (1999) 1.
- [27] R.A. Young, The Rietveld Method, International Union of Crystallography, Oxford University Press, 1995.
- [28] A.G. Belous, O.I. V'yunov, E.V. Pashkova, O.Z. Yanchevskii, A.I. Tovstolytkin, A.M. Yanchevskii, Inorg. Mater. 39 (2003) 212.
- [29] I.G. Krogh Andersen, E. Krogh Andersen, P. Norby, E. Scou, J. Solid State Chem. 113 (1994) 326.
- [30] R.J.H. Voorhoeve, in: J.J. Burton, R.L. Garten (Ed.), Advanced Materials in Catalysis, Academic Press, New York, 1977, p. 129.
- [31] A.K. Ladavos, P.J. Pomonis, Appl. Catal. B 1 (1992) 101.
- [32] Y. Teraoka, H. Nii, S. Kagawa, K. Jansson, M. Nygren, J. Mater. Chem. 6 (1) (1996) 97.
- [33] A.A. Leontiou, A.K. Ladavos, P.J. Pomonis, Appl. Catal. A 241 (2003) 133–141.
- [34] B.K. Cho, B.H. Shanks, J.E. Bailey, J. Catal. 113 (1989) 486.
- [35] The relevant program is available on request from the authors.
- [36] Y. Bard, Non Linear Parameter Estimation, Academic Press, New York, 1973, p. 83.

- [37] D. Cuthbert, F. Wood, J. Gorman, *Fitting Equations to Data: Computer Analysis of Multifactor Data*, Second ed., John Wiley & Sons, New York, 1999.
- [38] N. Matthes, D. Schweich, B. Martin, F. Castagna, *Top. Catal.* 16–17 (2001) 19.
- [39] G.C. Koltsakis, P.A. Konstantinidis, A.M. Stamatelos, *Appl. Catal. B: Environ.* 12 (1997) 161.
- [40] M.A. Pena, J.M.D. Tascon, L. Gonzalez Tejuca, *Nouv. J. Chim.* 9 (1985) 591.
- [41] A. Vannice, T. Yamashita, *Appl. Catal. B: Environ.* 13 (1997) 141.
- [42] S.-J. Huang, A.B. Walters, M.A. Vannice, *Appl. Catal. B: Environ.* 17 (1998) 183.
- [43] H.C. Yao, M. Shelef, *J. Phys. Chem.* 78 (1974) 2490.